Phase distortions in sum- and difference-frequency mixing in crystals

Arlee V. Smith

Lasers, Optics, & Remote Sensing Department, Sandia National Laboratories, Albuquerque, New Mexico 87185–0601

Mark S. Bowers

Aculight Corporation, Suite 100, 40 Lake Bellevue, Bellevue, Washington 98005

Received May 19, 1994; accepted July 17, 1994; revised manuscript received August 25, 1994

We show that if two waves are incident on a quadratically nonlinear crystal, with the third wave generated entirely within the crystal, a phase-velocity mismatch ($\Delta k \neq 0$) leads to intensity-dependent phase shifts of the generated wave only if there is walk-off, linear absorption, or significant diffraction of at least one of the waves as well as significant energy exchange among the waves. The result is frequency broadening and wave-front distortion of the generated wave. Although the induced phase distortions are usually quite small, they may be significant in applications that require high spectral resolution or pointing accuracy.

1. INTRODUCTION

In the limit of low mixing efficiency, three-wave mixing in a quadratically nonlinear medium has been described analytically. For lowest-order Gaussian beam profiles, Boyd and Kleinman[1] presented such a treatment, including walk-off and diffraction. In this weak mixing limit the phase profiles of the output waves are independent of the beam intensities. When energy exchange becomes significant we might expect the output phases to depend on the strength of the mixing, which is determined in part by the input intensities. In this case analytical solutions for the full problem with walk-off, diffraction, and depletion are not available. However, recent experiments and analyses of second-harmonic generation have shown[2–5] that, when energy exchange is significant, a phase-velocity mismatch ($\Delta k \neq 0$) among the interacting waves does indeed lead to intensity-dependent phase shifts of the fundamental wave. In some respects these phase shifts mimic those induced by an intensity-dependent refractive index, causing self-focusing or self-defocusing.[3] This raises the question whether there is a similar intensity-dependent shift in the phase of the second-harmonic wave that could lead to distortions of its wave front and, for pulsed light, to frequency chirps. Such effects could cause line-shape distortions in high-resolution spectra under some conditions. They could also cause time-dependent steering of the second-harmonic beam.

Here we consider the effects of phase-velocity mismatch in three-wave sum- and difference-frequency mixing in nonlinear crystals for pulse durations of a few nanoseconds. We consider only cases of moderate nonlinear drive such as might be encountered when one is striving for efficient frequency conversion with good output beam quality. We show that, when diffraction, walk-off, absorption, and group-velocity mismatch are insignificant, and only two waves are incident upon the crystal, the generated third wave will not acquire an intensity-dependent phase shift, apart from possible 180-deg phase reversals. All the phase distortion introduced by phase-velocity mismatch will show up in the two waves that had nonzero input intensity. If diffraction, walk-off, or absorption becomes important, or if all three waves are incident upon the crystal, this is no longer true. The output phases of all three waves will vary with the input intensities. Combined with spatial and temporal intensity variations of the input beams, this intensity dependence produces frequency shifts and wave-front distortions for all three waves.

First we will consider plane waves and the influence of linear absorption, input amplitudes, and input phases on the output phases. Then, to illustrate the phase distortions introduced by walk-off, we will present results from a numerical model of nonlinear mixing that includes spatial and temporal beam profiles, birefringence, linear absorption, diffraction, and phase-velocity mismatch. The model also permits significant energy exchange among the three waves.

2. EXACT PLANE-WAVE SOLUTIONS

The equations that describe the nonlinear interaction for plane waves in SI units are[6]

$$\frac{d\varepsilon_s}{dz} = i\frac{d_{\text{eff}}}{c}\frac{\omega_s}{n_s}\varepsilon_p\varepsilon_i^* \exp(i\Delta kz) - \alpha_s\varepsilon_s,$$

$$\frac{d\varepsilon_i}{dz} = i\frac{d_{\text{eff}}}{c}\frac{\omega_i}{n_i}\varepsilon_p\varepsilon_i^* \exp(i\Delta kz) - \alpha_i\varepsilon_i,$$

$$\frac{d\varepsilon_p}{dz} = i\frac{d_{\text{eff}}}{c}\frac{\omega_p}{n_p}\varepsilon_s\varepsilon_i \exp(-i\Delta kz) - \alpha_p\varepsilon_p, \qquad (1)$$

where the electric field E_ω at frequency ω is given by

$$E_\omega = \tfrac{1}{2}\{\varepsilon_\omega \exp[-i(\omega t - kz)] + \varepsilon_\omega^* \exp[i(\omega t - kz)]\}, \qquad (2)$$

the phase velocity mismatch Δk is defined by

0740-3224/95/010049-09$06.00

$$\Delta k = k_p - k_s - k_i\,, \tag{3}$$

and

$$\omega_p = \omega_s + \omega_i\,. \tag{4}$$

The subscripts p, s, and i refer to the pump, signal, and idler waves, respectively, as is customary. The coefficients d_{eff} and α are the effective nonlinear mixing coefficient and the linear absorption coefficient, respectively. Following the method of solution given by Armstrong *et al.*,[7] we write the fields as

$$\varepsilon_n = \epsilon_n \exp(i\vartheta_n)\,, \tag{5}$$

where the ϵ's are real valued. The mixing equations become

$$\begin{aligned}
\frac{\mathrm{d}\epsilon_s}{\mathrm{d}z} &= -\epsilon_p\epsilon_i \frac{d_{\text{eff}}}{c}\frac{\omega_s}{n_s}\sin\theta - \alpha_s\epsilon_s\,,\\
\frac{\mathrm{d}\epsilon_i}{\mathrm{d}z} &= -\epsilon_p\epsilon_s \frac{d_{\text{eff}}}{c}\frac{\omega_i}{n_i}\sin\theta - \alpha_i\epsilon_i\,,\\
\frac{\mathrm{d}\epsilon_p}{\mathrm{d}z} &= +\epsilon_s\epsilon_i \frac{d_{\text{eff}}}{c}\frac{\omega_p}{n_p}\sin\theta - \alpha_p\epsilon_p\,,\\
\frac{\mathrm{d}\vartheta_s}{\mathrm{d}z} &= \frac{d_{\text{eff}}}{c}\frac{\omega_s}{n_s}\frac{\epsilon_p\epsilon_i}{\epsilon_s}\cos\theta\,,\\
\frac{\mathrm{d}\vartheta_i}{\mathrm{d}z} &= \frac{d_{\text{eff}}}{c}\frac{\omega_i}{n_i}\frac{\epsilon_p\epsilon_s}{\epsilon_i}\cos\theta\,,\\
\frac{\mathrm{d}\vartheta_p}{\mathrm{d}z} &= \frac{d_{\text{eff}}}{c}\frac{\omega_p}{n_p}\frac{\epsilon_s\epsilon_i}{\epsilon_p}\cos\theta\,,
\end{aligned} \tag{6}$$

where θ is defined by

$$\theta = \vartheta_p - \vartheta_i - \vartheta_s + \Delta k z\,. \tag{7}$$

If the linear absorptions are all zero, the solution for θ given by Armstrong *et al.*[17] is

$$\cos\theta = \frac{\left(\Gamma - \dfrac{c\Delta k n_p \epsilon_p{}^2}{2d_{\text{eff}}\omega_p}\right)}{\epsilon_s\epsilon_i\epsilon_p}\,, \tag{8}$$

where Γ is an integration constant.

It can be shown that, if $\epsilon_i(z=0)$ and $\alpha_i = \alpha_s + \alpha_p$,

$$\cos\theta = \frac{\Delta k c}{2d_{\text{eff}}}\frac{n_i}{\omega_i}\frac{\epsilon_i}{\epsilon_s\epsilon_p} \tag{9}$$

is the solution for θ. Similarly, if $\epsilon_p(z=0)=0$ and $\alpha_p = \alpha_i + \alpha_s$,

$$\cos\theta = -\frac{\Delta k c}{2d_{\text{eff}}}\frac{n_p}{\omega_p}\frac{\epsilon_p}{\epsilon_s\epsilon_i} \tag{10}$$

is the solution. Thus, if the idler starts with zero intensity, from Eqs. (6) the equation for the idler phase becomes

$$\frac{\mathrm{d}\vartheta_i}{\mathrm{d}z} = +\frac{\Delta k}{2}\,. \tag{11}$$

This means that the phase of the idler wave is shifted relative to that of a solo idler wave by $+\Delta k z/2$ but is independent of the intensities of the three interacting waves.

We should point out that, although the idler phase is correctly given by Eq. (11), the amplitude ϵ_i can change sign if the mixing is strong enough to deplete the idler wave totally. When this occurs it results in an apparent abrupt 180° phase shift as the amplitude ϵ_i passes through zero. Because Eqs. (6) are symmetric in signal and idler, our discussion for the idler applies equally to the signal.

If the pump-wave intensity starts from zero, the equation for the pump phase becomes

$$\frac{\mathrm{d}\vartheta_p}{\mathrm{d}z} = -\frac{\Delta k}{2}\,, \tag{12}$$

and the pump phase is independent of the intensities of the three waves.

If the linear losses do not satisfy $\alpha_i = \alpha_s + \alpha_p$ in the case where $\epsilon_i(z=0)=0$, the phase of the idler wave will vary with intensity. Similarly, if the condition $\alpha_p = \alpha_i + \alpha_s$ is violated for $\epsilon_p(z=0)=0$ the pump phase will be intensity dependent.

In contrast to the intensity independence of the output phase that we just demonstrated for a wave that starts with zero intensity, if Δk is nonzero and the wave starts with nonzero intensity its input phase cannot be adjusted to make its output phase independent of the input intensities. We show this for the idler wave by combining Eq. (8) with the expression for $\mathrm{d}\vartheta_i/\mathrm{d}z$ in Eqs. (6) to get

$$\begin{aligned}
\frac{\mathrm{d}\vartheta_i}{\mathrm{d}z} = \frac{d_{\text{eff}}\omega_i}{cn_i\epsilon_i{}^2}\Bigg\{&\epsilon_i(0)\epsilon_s(0)\epsilon_p(0)\cos\theta(0)\\
&+ \frac{\Delta k c n_p}{2d_{\text{eff}}\omega_p}\left[\epsilon_p{}^2(0) - \epsilon_p{}^2\right]\Bigg\}\,.
\end{aligned} \tag{13}$$

Applying the Manley–Rowe relation

$$\frac{n_i}{\omega_i}\left[\epsilon_i{}^2 - \epsilon_i{}^2(0)\right] = \frac{n_p}{\omega_p}\left[\epsilon_p{}^2(0) - \epsilon_p{}^2\right] \tag{14}$$

yields, for Eq. (13),

$$\begin{aligned}
\frac{\mathrm{d}\vartheta_i}{\mathrm{d}z} = \frac{d_{\text{eff}}\omega_i}{cn_i\epsilon_i{}^2}\Bigg[&\epsilon_s(0)\epsilon_i(0)\epsilon_p(0)\cos\theta(0)\\
&- \frac{\Delta k c n_i}{2d_{\text{eff}}\omega_i}\epsilon_i{}^2(0)\Bigg] + \frac{\Delta k}{2}\,.
\end{aligned} \tag{15}$$

The idler output phase will be independent of the idler intensity only if the first term on the right-hand side in Eq. (15) is also independent of the idler intensity. This requires that the quantity in brackets be zero, i.e., that

$$\cos\theta(0) = \frac{\Delta k c n_i}{2d_{\text{eff}}\omega_i}\frac{\epsilon_i(0)}{\epsilon_s(0)\epsilon_p(0)}\,. \tag{16}$$

For any set of input intensities the idler input phase could be adjusted to meet this condition. However, this input phase would depend on the input intensities, violating the goal of intensity independence. Thus there is no single choice of input idler phase that allows the output idler phase to be intensity independent. If all three waves have nonzero incident intensity, all three output phases vary with input intensity.

To summarize, we have shown that, for plane waves with no linear absorption, if one wave enters the crystal

with zero intensity its output phase will be independent of the intensities of the input waves and will depend only on ΔkL, where L is the crystal length. The output phases of the other two waves will be intensity dependent if $\Delta k \neq 0$. If there is linear absorption the phase of the wave that started with zero intensity will also become intensity dependent for $\Delta k \neq 0$, unless a special condition of the absorption coefficients is met ($\alpha_i = \alpha_s + \alpha_p$ or $\alpha_p = \alpha_i + \alpha_s$). If the third wave enters the crystal with nonzero intensity, its input phase cannot be adjusted to make its output phase intensity independent if $\Delta k \neq 0$.

Clearly, when $\Delta k \neq 0$, the intensity independence of the output phase of one wave is satisfied only in the special circumstance that the wave starts with zero intensity. It is also necessary that the balance of amplitudes and phases of the three interacting waves as they progress through the crystal not be altered from that of plane waves interacting without loss (or meeting the special loss criterion). These results were derived for plane waves. In the remainder of this paper we consider waves that are spatially and temporally nonuniform. In that case, effects that upset the special balance required for an intensity-independent output phase include different rates of diffractive spreading for the three waves, group-velocity mismatch among the waves, and walk-off among the three waves. If any of these effects is strong enough that the plane-wave approximation is invalid, and if $\Delta k \neq 0$, we expect the phases of all three waves at the crystal output face to depend on the input intensities. The phases will vary in space and time, leading to frequency chirps and wavefront distortions for all three waves. Furthermore, even if Δk is nominally zero, we expect walk-off to lead to intensity-dependent output phases for all three waves if the beams have diameters small enough that diffractive phase shifts are significant. The explanation is that the diffractive phase slippage mimics nonzero Δk. Alternatively, one can argue that small-diameter beams consist of a sum of plane waves with a range of transverse k-vector components, so Δk is not truly zero for nonlinear interactions among many contributions of the plane-wave components.

3. NUMERICAL MODELING WITH NONUNIFORM SPATIAL AND TEMPORAL PROFILES

Our discussion of output phases for nonuniform beams was based on plane-wave interactions and was by necessity qualitative in nature because analytic solutions of the mixing equations that include all the effects important for nonuniform beams are not available. To achieve quantitative results we must resort to numerical modeling when we include the effects of nonzero Δk in the presence of birefringence and large energy exchange among the three mixing waves.

We have developed a time-dependent model of three-wave mixing that numerically integrates the three wave equations with the inclusion of walk-off and diffraction in the paraxial approximation. The model describes the stepwise time evolution of each beam on a two-dimensional spatial grid of intensity and phase. We assume Gaussian spatial and temporal input profiles for the three beams. The integration of the three wave equations through the nonlinear crystal is performed by use of Fourier-transform techniques, as for the method described by Dreger and McIver.[8] When nonuniform transverse profiles are considered and the transverse derivatives are kept in the wave equations in order to account for walk-off and diffraction, the equations that replace Eqs. (1) take the form

$$\frac{\partial \varepsilon_j(x, y, z, t)}{\partial z} = \frac{i}{2k_j}\left[\frac{\partial^2 \varepsilon_j(x, y, z, t)}{\partial y^2} + \frac{\partial^2 \varepsilon_j(x, y, z, t)}{\partial x^2}\right] - \tan\rho\,\frac{\partial \varepsilon_j(x, y, z, t)}{\partial x} + P_j(x, y, z, t) - \alpha_j \varepsilon_j(x, y, z, t), \tag{17}$$

where j is the frequency index and ρ is the walk-off angle in the x direction. For ordinary or y-polarized light, ρ is zero. For extraordinary or x-polarized light, ρ is the walk-off angle appropriate for the crystal orientation of interest. We have ignored the small anisotropy in the diffractive term for extraordinary waves propagating in a birefringent crystal.[8] P_j is the polarization term at frequency ω_j and is given by

$$\begin{aligned} P_s(x, y, z, t) &= i\,\frac{d_{\text{eff}}}{c}\,\frac{\omega_s}{n_s}\,\varepsilon_p(x, y, z, t) \times \varepsilon_i^*(x, y, z, t)\exp(i\Delta k z), \\ P_i(x, y, z, t) &= i\,\frac{d_{\text{eff}}}{c}\,\frac{\omega_i}{n_i}\,\varepsilon_p(x, y, z, t) \times \varepsilon_s^*(x, y, z, t)\exp(i\Delta k z), \\ P_p(x, y, z, t) &= i\,\frac{d_{\text{eff}}}{c}\,\frac{\omega_p}{n_p}\,\varepsilon_i(x, y, z, t) \times \varepsilon_s(x, y, z, t)\exp(-i\Delta k z). \end{aligned} \tag{18}$$

Fourier transforming the electric fields and polarizations in the transverse dimension, using

$$\begin{aligned} \varepsilon_j(x, y, z, t) &= \int_{-\infty}^{\infty}\int_{-\infty}^{\infty} \varepsilon_j(s_x, s_y, z, t) \times \exp[i2\pi(s_x x + s_y y)]\mathrm{d}s_x \mathrm{d}s_y, \\ P_j(x, y, z, t) &= \int_{-\infty}^{\infty}\int_{-\infty}^{\infty} P_j(s_x, s_y, z, t) \times \exp[i2\pi(s_x x + s_y y)]\mathrm{d}s_x \mathrm{d}s_y, \end{aligned} \tag{19}$$

and substituting these definitions of $\varepsilon_j(x, y, z, t)$ and $P_j(x, y, z, t)$ into Eq. (17), we arrive at the following equation for the propagation of the individual spatial-frequency component waves:

$$\frac{\partial \varepsilon_j(s_x, s_y, z, t)}{\partial z} = -i\left[\frac{2\pi^2}{k_j}(s_x^2 + s_y^2) + 2\pi s_y \tan\rho\right] \times \varepsilon_j(s_x, s_y, z, t) + P_j(s_x, s_y, z, t). \tag{20}$$

This procedure results in three coupled first-order ordinary differential equations for the change in each spatial-frequency component of the fields as they propagate through the crystal. The equations are coupled through the nonlinear interaction term $P_j(s_x, s_y, z, t)$.

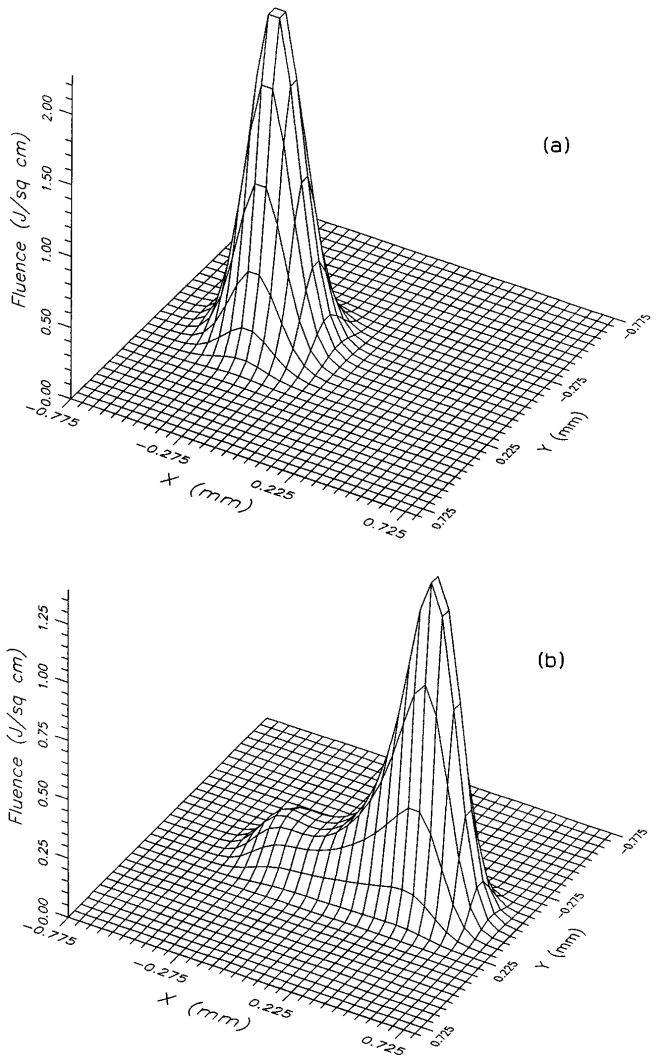

Fig. 1. Example fluence profiles for (a) the input fundamental wave and (b) the output second-harmonic wave. The second-harmonic wave walks off in the $+x$ direction. $\Delta k = 0.15\ \mathrm{mm}^{-1}$.

We model the mixing process for each time step by propagating half of a z step, using a Runge–Kutte algorithm to numerically integrate the coupled ordinary differential equations. We then apply a fast-Fourier-transform algorithm to transform the resulting spatial-frequency fields $\varepsilon_j(s_x, s_y, z, t)$ into fields $\varepsilon_j(x, y, z, t)$ in x–y space. We insert these fields into Eqs. (18) to find $P_j(x, y, z, t)$. We then apply the fast-Fourier transform algorithm again to obtain the $P_j(s_x, s_{yz}, z, t)$'s, which are used in Eq. (20) to propagate the second half of the z step.

The x–y spatial grid is typically 32×32, and the integration of a single time slice through the crystal is performed in approximately 32 steps. The number of time slices is typically approximately 75. Run time on a Pentium PC is of the order of 1000 s. As described previously,[9] we have rigorously validated the model by comparison with experiments.

We will focus our discussion on two examples. In the first, we model a situation in which birefringence is combined with nonzero Δk. In the second, birefringence is combined with significant diffraction but with $\Delta k = 0$.

Case 1: Nonzero Phase Mismatch with Birefringence

The first case is one that has been experimentally studied by Gangopadhyay *et al.*[10] They frequency doubled 3.4-mJ 7-ns (FWHM) pulses of 645-nm light in a 3-cm-long KDP crystal. For this Type I doubling, the 645-nm light had ordinary polarization. The 322.5-nm light had extraordinary polarization and a walk-off, or birefringent, angle of 28 mrad. The input beam diameter (FWHM) was 0.25 mm. For this process, $d_{\mathrm{eff}} = 0.32$ pm/V. They measured second-harmonic conversion efficiency and phase shifts for $\Delta k = 0$ and $\Delta k = 0.15\ \mathrm{mm}^{-1}$.

Because the input beam diameter is quite large, diffraction is insignificant for this case (the Rayleigh range[11] in the crystal is 33 cm). We have verified this by performing calculations with and without diffraction and obtaining identical results. We also neglect group-velocity mismatch as inconsequential. Figure 1 shows our calculated input fundamental [Fig. 1(a)] and output second-harmonic [Fig. 1(b)] fluence profiles for $\Delta k = 0.15\ \mathrm{mm}^{-1}$. Figure 2 displays the time development of the phase of the second-harmonic light at three spatial grid points, again for $\Delta k = 0.15\ \mathrm{mm}^{-1}$. At these three locations the phase of the second-harmonic wave clearly varies with the input intensity of the fundamental waves. If Δk is zero or if the walk-off is artificially set to zero we find that the phase of the second-harmonic light is constant in time and independent of the input fundamental intensity. These observations are consistent with our conclusions drawn from examining the plane-wave solutions above.

To characterize the wave-front distortions at an instant of time we calculate the tilt, curvature, and residual distortion of the output waves. In our notation, x is the walk-off direction and y is perpendicular to it. The tilt angle in the walk-off direction, β_x, is the first moment in the spatial-frequency domain, defined by

$$\beta_x(t) = \frac{-\lambda \int_{-\infty}^{\infty}\int_{-\infty}^{\infty} s_x |\varepsilon(s_x, s_y, t)|^2 \mathrm{d}s_x \mathrm{d}s_y}{\int_{-\infty}^{\infty}\int_{-\infty}^{\infty} |\varepsilon(s_x, s_y, t)|^2 \mathrm{d}s_x \mathrm{d}s_y}, \qquad (21)$$

where s_x and s_y are the transverse components of the spatial frequency and

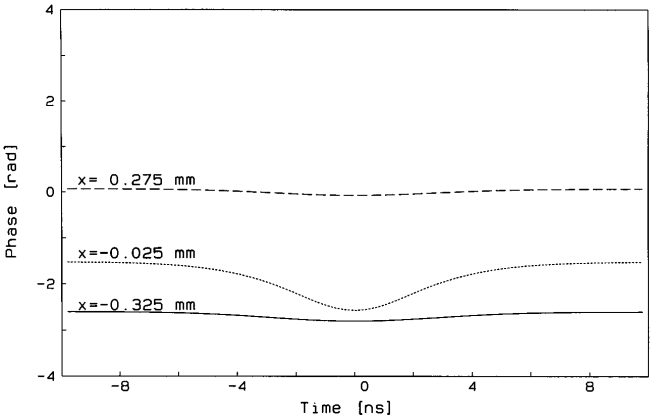

Fig. 2. Phases of the output second-harmonic optical field for $\Delta k = 0.15\ \mathrm{mm}^{-1}$ at three positions on the calculational grid. The y positions are zero, and the x positions are as labeled.

$$\varepsilon(s_x, s_y, t) = \int_{-\infty}^{\infty}\int_{-\infty}^{\infty} \varepsilon(x, y, t)\exp[-i2\pi(s_x x + s_y y)]\mathrm{d}x\mathrm{d}y. \tag{22}$$

The centroid of a beam's intensity propagates at the tilt angle β_x.

The cylindrical curvature of the wave fronts in the plane of walk-off and perpendicular to it is characterized by use of methods similar to those described by Siegman.[12] The number of waves of curvature is

$$c_x(t) = \frac{{\sigma_x}^2(t)}{\lambda R_x(t)}, \tag{23}$$

where

$$R_x(t) = Z_x(t)\left[1 + \frac{{\sigma_{\mathrm{ox}}}^2(t)}{\lambda^2 {\sigma_{s_x}}^2(t) {Z_x}^2(t)}\right]. \tag{24}$$

The z positions of the x-dimension beam waist, $Z_x(t)$, and the waist size, $\sigma_{\mathrm{ox}}(t)$, are given by

$$Z_x(t) = \frac{A_x(t) + 2\beta_x(t)\overline{x}(t)}{2\lambda^2 {\sigma_{s_x}}^2(t)}, \tag{25}$$

$${\sigma_{\mathrm{ox}}}^2(t) = {\sigma_{\mathrm{ox}}}^2(t) - {Z_x}^2(t)\lambda^2 {\sigma_{s_x}}^2(t). \tag{26}$$

$Z_x(t)$ is measured relative to the plane where $A_x(t)$ and $\overline{x}(t)$ are specified. $\overline{x}(t)$ is the x position of the intensity centroid:

$$\overline{x}(t) = \frac{\int_{-\infty}^{\infty}\int_{-\infty}^{\infty} x|\varepsilon(x, y, t)|^2\mathrm{d}x\mathrm{d}y}{\int_{-\infty}^{\infty}\int_{-\infty}^{\infty} |\varepsilon(x, y, t)|^2\mathrm{d}x\mathrm{d}y}. \tag{27}$$

$A_x(t)$ is

$$A_x(t) = \frac{i\lambda}{2\pi}\frac{\int_{-\infty}^{\infty}\int_{-\infty}^{\infty} s_x\left[\varepsilon(s_x, s_y, t)\frac{\partial\varepsilon^*(s_x, s_y, t)}{\partial s_x} - \mathrm{c.c.}\right]\mathrm{d}s_x\mathrm{d}s_y}{\int_{-\infty}^{\infty}\int_{-\infty}^{\infty} |\varepsilon(s_x, s_y, t)|^2\mathrm{d}s_x\mathrm{d}s_y}; \tag{28}$$

$${\sigma_x}^2(t) = \frac{\int_{-\infty}^{\infty}\int_{-\infty}^{\infty} [x - \overline{x}(t)]^2|\varepsilon(x, y, t)|^2\mathrm{d}x\mathrm{d}y}{\int_{-\infty}^{\infty}\int_{-\infty}^{\infty} |\varepsilon(x, y, t)|^2\mathrm{d}x\mathrm{d}y}, \tag{29}$$

$${\sigma_{s_x}}^2(t) = \frac{\int_{-\infty}^{\infty}\int_{-\infty}^{\infty} [\lambda s_x - \beta_x(t)]^2|\varepsilon(s_x, s_y, t)|^2\mathrm{d}s_x\mathrm{d}s_y}{\lambda^2\int_{-\infty}^{\infty}\int_{-\infty}^{\infty} |\varepsilon(s_x, s_y, t)|^2\mathrm{d}s_x\mathrm{d}s_y}. \tag{30}$$

After tilt and cylindrical curvature are accounted for, the remaining distortion is characterized by two values of Siegman's[13] M^2. One, ${M_x}^2$, is calculated in the walk-off plane, and the other, ${M_y}^2$, is calculated in the plane perpendicular to walk-off. The quantity ${M_x}^2$ is defined by

$${M_x}^2(t) = 4\pi\sigma_{\mathrm{ox}}(t)\sigma_{s_x}(t). \tag{31}$$

It is the product of the real-space variance and the spatial-frequency-space variance of intensity for an actual beam normalized to that for an ideal Gaussian beam. An M^2 of 1 corresponds to a Gaussian beam with no phase distortions. Any amplitude or phase distortion makes M^2 larger than unity.

Figure 3 compares the output powers, tilts, curvatures, and ${M_x}^2$'s for $\Delta k = 0$ with those for $\Delta k = 0.15\ \mathrm{mm}^{-1}$. Figures 3(a)–3(e) show results for $\Delta k = 0$, and Figs. 3(f)–3(j) show results for $\Delta k = 0.15\ \mathrm{mm}^{-1}$. Figures 3(a) and 3(f) compare the power out of the crystal as a function of time for a Gaussian input pulse profile (7 ns FWHM). The calculated mixing efficiencies, defined as 322.5-nm energy out divided by 645-nm energy in, are 0.56 and 0.37 for these two cases. These are larger than the measured efficiencies[10] of 0.36 and ~0.18. This discrepancy is probably due to differences between the experimental and model beams. Figures 3(b) and 3(g) compare the tilts in the walk-off, or x, direction. For $\Delta k = 0$ there is no tilt of either the fundamental or the second-harmonic beam. For $\Delta k = 0.15\ \mathrm{mm}^{-1}$ the second-harmonic wave tilts in the direction of walk-off, and the fundamental wave tilts by nearly an equal amount in the opposite direction, with pronounced intensity dependence. These tilts reverse sign if the sign of Δk is reversed. Tilts in the y direction are zero for all values of Δk.

The cylindrical curvatures shown in Figs. 3(c) and 3(h) indicate that there is no curvature for $\Delta k = 0$, whereas there are intensity-dependent curvatures for $\Delta k = 0.15\ \mathrm{mm}^{-1}$. At the peak of the pulse the fundamental beam is slightly diverging at the crystal exit face, and the second-harmonic beam is slightly converging.

The calculated values of ${M_x}^2$ are plotted in Figs. 3(d) and 3(i). For low input intensities near the beginning and the end of the pulse, ${M_x}^2$ for the fundamental wave is unity, as it must be for the input Gaussian transverse profile. The second-harmonic wave's ${M_x}^2$ is greater than 1 because of the walk-off-induced elongation of its beam profile. Notice that the values of ${M_x}^2$ increase with intensity in each case and that the increase is more pronounced for $\Delta k \neq 0$.

The time-varying tilts, curvatures, and residual distortions just discussed are the consequence of intensity-dependent output phases similar to those displayed in Fig. 2. Another consequence of this time variation must be frequency chirps and shifts. These could be measured in two ways. One is to heterodyne the output beam with a frequency-shifted reference beam as Gangopadhyay *et al.*[10] did. This can reveal phase shifts much smaller than 1 rad over any selected part of the beam. By its nature, this technique measures $[\int \varepsilon_{\mathrm{ref}}^*\varepsilon(t)\mathrm{d}A + \mathrm{c.c.}]$, that is, the electric field weighted by the reference field and integrated over an area. In our modeling we simulate this measurement by summing the output electric field over the spatial grid at each time step and calculate the phase of this summed field as a function of time.

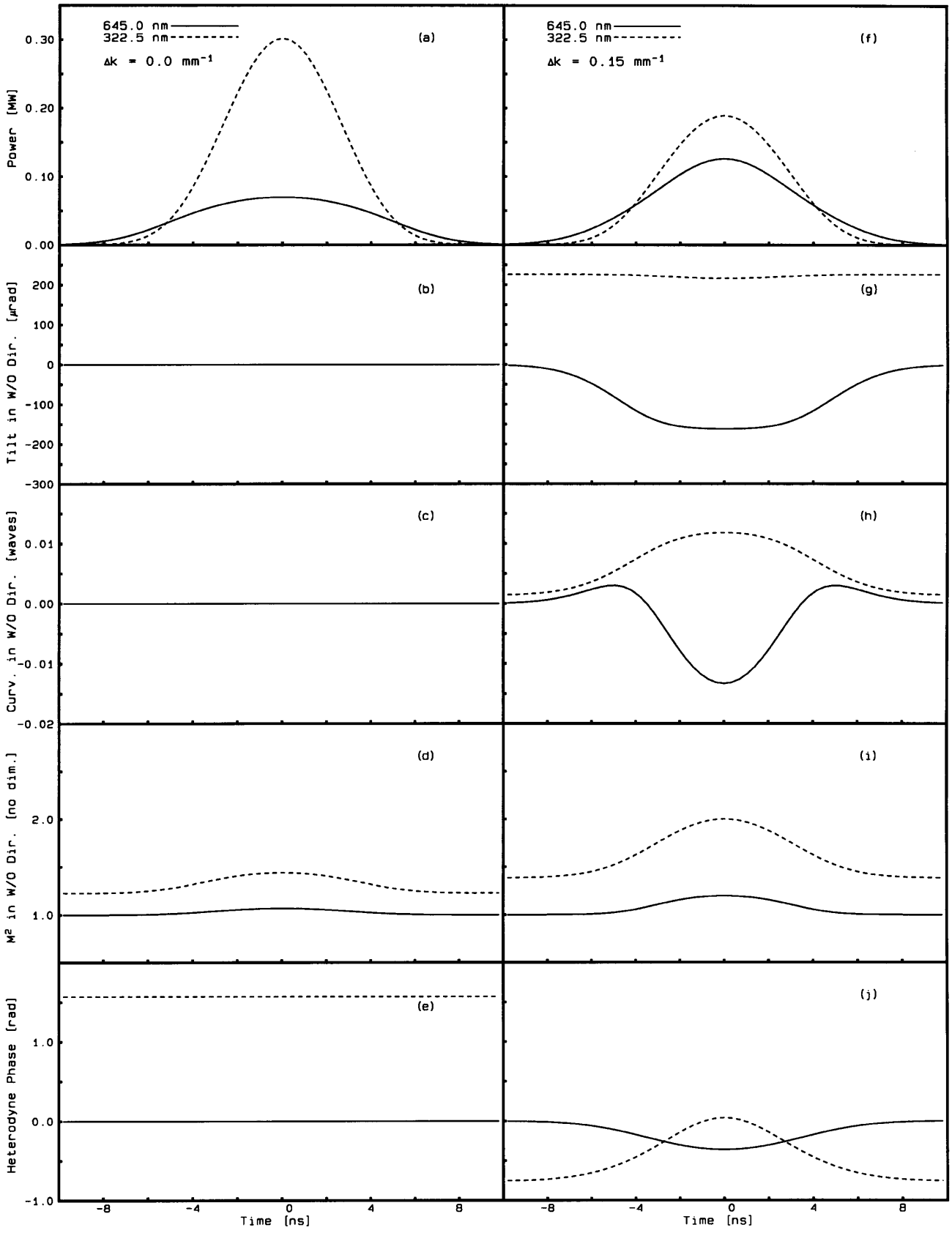

Fig. 3. Numerical results for frequency doubling a 7-ns (FWHM Gaussian), 0.25-mm-diameter (FWHM lowest-order Gaussian) pulse of 645-nm light in a 3-cm-long KDP crystal. The conditions are described for Case 1 in the text. Results for (a)–(e) $\Delta k = 0$, (f)–(j) $\Delta k = 0.15\ \mathrm{mm}^{-1}$. In (a) and (f) the solid curve is one half of the 645-nm power and the dashed curve is the full 322.5-nm power. The tilt, curvature, and M^2 characterize the wave-front distortions in the walk-off direction. The heterodyne phases of the depleted fundamental and generated second harmonic are at the exit face of the crystal.

An alternative method of measuring the frequency spectrum is to use a square-law-detection apparatus such as a spectrometer mated to an intensity monitor. We simulate this measurement by calculating the Fourier time transform of the field at each spatial grid point and summing the transforms weighted by the pulse energy at each grid point. As we will see, these two measurement methods can produce quite different results.

Using the latter method with $\Delta k = 0$, we find that the fundamental and the second-harmonic spectra are virtually identical to Fourier transforms of the power profiles shown in Fig. 3(a). For $\Delta = 0.15\ \mathrm{mm}^{-1}$ the time variation of the phase shown in Fig. 2 suggests there will be frequency chirps and broadening of the spectra relative to the power profile transforms. Indeed, comparing the square-law spectra with these transforms reveals that there is some broadening, but it adds less than 2 MHz to the width (FWHM) of the fundamental and second-harmonic spectra. We attribute the broadening of the second-harmonic spectrum to a small blue shift on the leading edge of the pulse followed by an equal red shift on the trailing edge, as suggested by Fig. 2.

Figures 3(e) and 3(j) display the heterodyne phases. As Fig. 3(e) shows, there are no phase shifts for $\Delta k = 0$. For $\Delta k = 0.15\ \mathrm{mm}^{-1}$ the heterodyne phase of the fundamental decreases with increasing intensity, whereas the phase of the second-harmonic wave shifts in the opposite direction. The maximum apparent second-harmonic and fundamental frequency shifts are ~30 and ~15 MHz, respectively.

Gangopadhyay *et al.*[10] measured heterodyne phases of the second-harmonic wave as a function of time for $\Delta k = 0$ and $\Delta k = 0.15\ \mathrm{mm}^{-1}$. For $\Delta k = 0.15\ \mathrm{mm}^{-1}$ they found that the second harmonic appeared to be red shifted by ≈20 MHz on the leading edge of the pulse and blue shifted by ≈10 MHz on the falling edge compared with those in the $\Delta k = 0$ case. Unfortunately, the sign of Δk was not recorded, and the error bars for the measurement are nearly as large as the shifts, so detailed comparison of their measurement with our calculation is impossible.

The calculated and measured heterodyne phases might be interpreted as a 30-MHz red shift followed by an equal blue shift for the second-harmonic light and a 15-MHz blue shift followed by an equal red shift for the fundamental light. However, these conclusions would be at odds with the square-law spectra. For the second-harmonic wave the frequency shifts have the opposite sign from those deduced from examination of the phases of individual spatial-grid points shown in Fig. 2, which we used to calculate the square-law spectra. In addition, the frequency shifts deduced from heterodyne phases are much larger than those seen in the square-law spectra.

The cause of this apparent paradox is the combination of beam tilt with a shift in the centroid of the beams in the walk-off dimension. Because we assume that the detector is very close to the output face of the crystal, tilt alone will not cause the calculated behavior of the heterodyne phases. It will merely weaken the heterodyne signal by producing fringes on the detector face where the wave interferes with the tilt-free reference wave. In our case there is only a fraction of a fringe, so this should not be an important effect. However, the existence of a tilt toward the walk-off direction for the second-harmonic wave implies that the phase of this wave must increase on scanning from $-x$ to $+x$. As Fig. 3(g) shows, the tilt of the second harmonic is relatively constant throughout the pulse, so the second-harmonic phase fronts are nearly stationary, apart from higher-order distortions. However, the centroid of the second-harmonic beam scans from $-x$ to $+x$ as its intensity increases. This movement of the centroid is due to fundamental wave depletion. As Fig. 1 shows, the second-harmonic output beam is quite elongated in the walk-off direction because the maximum walk-off of 0.84 mm is large compared with the input beam diameter of 0.25 mm. The part of the beam displaced the most was generated near the input face of the crystal, whereas the part displaced the least was generated near the exit face. For low input intensities the fundamental wave is not significantly depleted, so the second-harmonic wave's intensity is quite uniform over its elongated profile. Its centroid is at $x = 0.42$ mm, i.e., shifted in the walk-off direction by half the product of the walk-off angle and the crystal length. As the input fundamental intensity increases, it generates second-harmonic light efficiently near the input face of the crystal but becomes depleted part way through the crystal, thus generating less second-harmonic output near the exit face. Consequently the second-harmonic output beam is brightest on the walk-off side. Its centroid shifts in the walk-off direction as the fundamental intensity increases. Because the walk-off direction is also the direction of increased phase owing to the tilt of the second-harmonic wave, and because the heterodyne phase is weighted by the field amplitude, this combination of nearly constant tilt and shifting centroid explains the positive second-harmonic-wave heterodyne phase shift with increasing intensity. This effect is smaller for the fundamental wave because its walk-off angle is zero so its centroid shifts much less.

The conclusion is that the heterodyne measurement of the second-harmonic wave is not necessarily a measure of the spectral shifts relevant for spectrometry. It is predominantly a measure of the tilt and the centroid shift of the wave. Indeed, the sign of the chirp measured by the heterodyne method for the second-harmonic wave is much larger than and opposite in direction to that of the chirp that would be seen by a collection of atoms. Clearly, this conclusion is based on the choice of a reference beam with zero tilt. Tilting the reference beam by 200 μrad to align it with the second-harmonic beam would dramatically alter the expected heterodyne phase. In addition, we calculated the heterodyne phases assuming infinite plane-wave reference beams, and the phases would be different if we used a reference beam matched more closely in size to the actual beams. However, the conclusion remains that its sensitivity to tilt makes it difficult to relate the heterodyne phase measurement to square-law-detector spectral measurements.

Case 2: Diffraction with Birefringence

This second example of numerical modeling illustrates the effect of diffraction combined with birefringence. As discussed above, we expect diffractive phase slippage to mimic phase-velocity mismatch and produce phase distortions of the generated wave even in the absence of a mismatch. We model the same system as in Case 1, except that here the crystal is shortened to 2 mm and

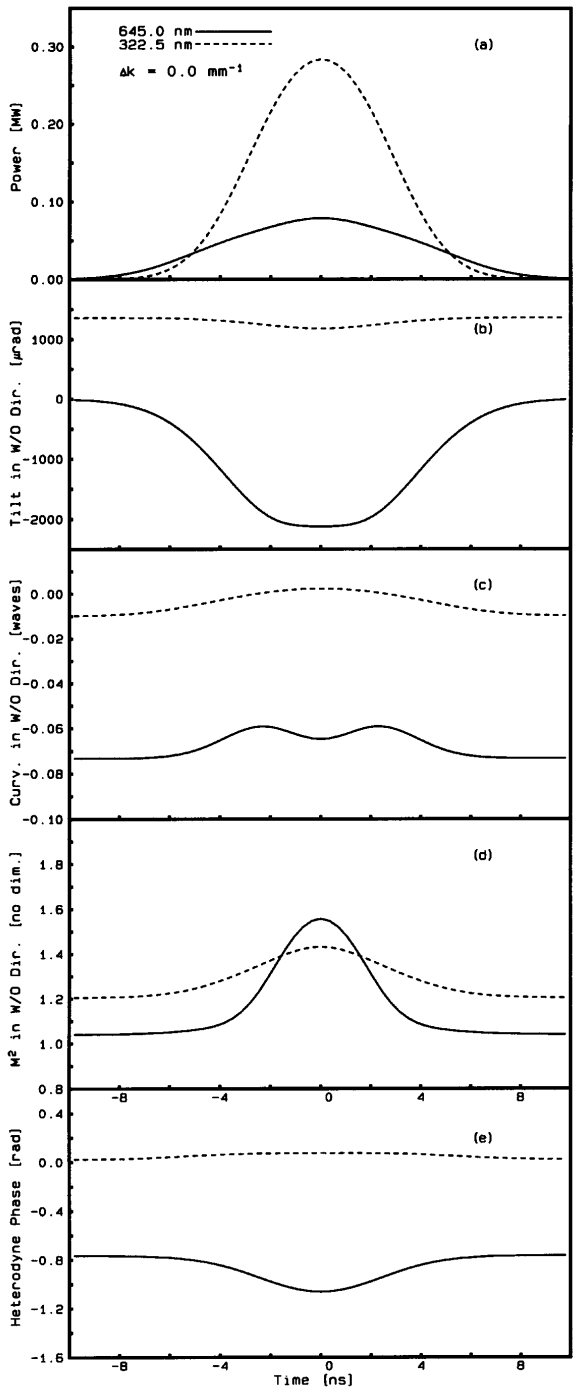

Fig. 4. Numerical results for frequency doubling a 7-ns (FWHM), 14-μm waist-diameter (FWHM) pulse of 645-nm light in a 2-mm-long KDP crystal with $\Delta k = 0$. The conditions are described for Case 2 in the text. In (a) the solid curve is one half of the 645-nm power and the dashed curve is the full 322.5-nm power. The tilt, curvature, and M^2 characterize the wave-front distortions in the walk-off direction. The heterodyne phases of the depleted fundamental and generated second harmonic are at the exit face of the crystal.

the fundamental beam is focused to a waist of 14 μm (FWHM of intensity) at the center of the crystal (Rayleigh range, 1 mm). This gives a conversion efficiency similar to that for $\Delta k = 0$ in Case 1 and also has the same beam-diameter-to-walk-off ratio. Figure 4 summarizes the results at the exit face of the crystal. The second-harmonic wave tilts toward the walk-off direction, and the fundamental wave tilts in the opposite direction. The tilts are much larger than for Case 1 but are still much less than the diffractive spread of the beams. Figure 4(c) shows that the fundamental wave at the crystal exit face is diverging early and late in the pulse because it is focused at the center of the crystal. The second-harmonic wave is substantially less divergent. Both beams diverge less at the peak of the pulse, and the second-harmonic wave has almost no net curvature. Figure 4(d) shows residual distortions or M^2's comparable with those of Case 1, but here the fundamental wave is distorted more than the second harmonic. The heterodyne phase shifts are quite small, as Fig. 4(e) shows, and the square-law spectra are noticeably different from the transform of the pulse envelopes only in the far wings of the fundamental spectrum.

4. CONCLUSIONS

We have shown that in the plane-wave approximation a wave starting from zero initial intensity in sum- or difference-frequency mixing in a quadratically nonlinear medium with nonzero Δk will suffer no intensity-dependent phase shifts. This lack of sensitivity to intensity is a special situation, however, and any upset of the balance of intensity or phase among the mixing waves is expected to introduce intensity-sensitive phase shifts. We illustrated this by numerically modeling a case in which the walk-off of one wave was comparable with the beam diameters, violating the plane-wave approximation. We showed that the resulting intensity-dependent phase shifts of the second-harmonic light produced frequency chirps for pulsed light, and also wave-front tilts, focusing, and other distortions. We also showed that heterodyne techniques are not a reliable means of measuring the spectral content of beams leaving a nonlinear mixing crystal. In a second example we showed that diffraction produces similar effects. Other situations that violate the plane-wave approximation and so can be expected to lead to beam distortions include mixing with crossed beams when the crossing angle is large enough that the beams separate by an amount comparable with their diameters, group-velocity mismatches large enough to displace the pulses by an amount comparable with their durations, and linear absorption of any wave (except in the special cases mentioned). The resulting distortions are generally small, but they may be significant when beam pointing or frequency stability is critical. The phase distortions may also become significant in optical parametric oscillators, for which phase distortions can accumulate over many transversals of the optical cavity.

ACKNOWLEDGMENTS

We thank W. J. Alford for helpful suggestions regarding this paper. This research is supported by U.S. Department of Energy under contract DE-AC04-94AL85000.

REFERENCES

1. G. D. Boyd and D. A. Kleinman, "Parametric interaction of focused Gaussian light beams," J. Appl. Phys. **39,** 3597–3639 (1968).

2. G. I. Stegeman, M. Sheik-Bahae, E. Van Stryland, and G. Ascend, "Large nonlinear phase shifts in second-order nonlinear-optical processes," Opt. Lett. **18,** 13–15 (1993).
3. R. DeSalvo, D. J. Hagar, M. Sheik-Bahae, G. Stegeman, and E. Van Stryland, "Self-focusing and self-defocusing by cascaded second-order effects in KTP," Opt. Lett. **17,** 28–30 (1992).
4. J.-M. R. Thomas and J.-P. E. Taran, "Pulse distortions in mismatched second harmonic generation," Opt. Commun. **4,** 329–333 (1972).
5. P. Pliszka and P. P. Banerjee, "Self-phase modulation in quadratically nonlinear media," J. Mod. Opt. **40,** 1909–1916 (1993); "Nonlinear transverse effects in second-harmonic generation," J. Opt. Soc. Am. B **10,** 1810–1819 (1993).
6. R. L. Byer and R. L. Herbst, "Parametric oscillation and mixing," in *Nonlinear Infrared Generation*, Y. R. Shen, ed. (Springer-Verlag, Berlin, 1977).
7. J. A. Armstrong, N. Bloebergen, J. Ducuin, and P. S. Pershan, "Interactions between light waves in a nonlinear dielectric," Phys. Rev. **127,** 1918–1939 (1962).
8. M. A. Dreger and J. K. McIver, "Second-harmonic generation in a nonlinear anisotropic medium with diffraction and depletion," J. Opt. Soc. Am. B **7,** 776–784 (1990).
9. T. D. Raymond, W. J. Alford, and A. V. Smith, "Frequency shifts in seeded optical parametric oscillators with phase mismatch," Bull. Am. Phys. Soc. **38,** 1715 (1993).
10. S. Gangopadhyay, N. Melikechi, and E. E. Eyler, "Optical phase perturbations in nanosecond pulsed amplification and second harmonic generation," J. Opt. Soc. Am. B **11,** 231–241 (1994).
11. A. E. Siegman, *Lasers* (University Science, Mill Valley, Calif., 1986).
12. A. E. Siegman, "Defining the effective radius of curvature for a nonideal optical beam," IEEE J. Quantum Electron. **27,** 1146–1148 (1991).
13. A. E. Siegman, "New developments in laser resonators," in *Optical Resonators*, D. A. Holmes, ed., Proc. Soc. Photo-Opt. Instrum. Eng. **1224,** 2–14 (1990).